

Modulation of acoustoelectric domains by intense 1.06- μm laser excitation of electrons in GaAs†

George K. Celler* and Ralph Bray

Physics Department, Purdue University, West Lafayette, Indiana 47907

(Received 30 October 1975)

Intense yttrium-aluminum-garnet laser pulses produce various strong modulation effects in acoustoelectric domains in n -GaAs at 300 K. The laser modulation of both the acoustoelectric current and phonon intensity has been studied. The response to the light pulses was greatly dependent on the stage in the evolution of the phonon domain. It was determined that the primary cause for the modulation of the acoustoelectric interaction was extrinsic excitation of electrons from deep traps, about 1.2 eV below the conduction band, which were present in concentrations of about 10^{16} cm^{-3} in our samples. A model is presented, based on small-signal acoustoelectric theory, which explains qualitatively all the diverse modulation effects in terms of the transiently increased electron concentration. According to this model, the modulation of current and phonon intensity is caused primarily by two factors: the change in the electron drift velocity in the domain which affects the acoustic gain and the change in the screening of the piezoelectric field which shifts the spectrum of the acoustoelectric interaction to higher phonon frequency. The controlled modulation of carrier concentration and drift velocity permit experimental clarification of the role of these parameters in the evolution of acoustoelectric domains.

I. INTRODUCTION

Propagating domains¹⁻⁵ of intense acoustic flux can be produced in piezoelectric semiconductors by acoustoelectric amplification of phonons from the thermal equilibrium background. *Passive* optical probing of such domains, primarily by Brillouin scattering of light by the amplified phonons, has served to elucidate the basic characteristics of such domains, including their shape, velocity, and the evolution of the strength and spectral distribution of the amplified acoustic flux.^{6,7} In the course of further domain studies⁸ in semiconducting GaAs, we found an *active* response to intense, Q -switched, YAlG: Nd laser light pulses at 1.06 μm , consisting of very strong modulation of the acoustoelectric current and the phonon intensity. Since the excitation in GaAs at 1.06 μm is extrinsic, very strong photoconductive effects were quite unexpected for semiconducting samples at room temperature. Furthermore, the maximum light intensity used, about 70 kW/cm², was much too low to invoke any appreciable excitation by nonlinear processes.⁹ Various diagnostic experiments revealed that the photoconductive modulation in the domain involved two factors:

(i) The primary effect of the intense radiation was to excite electrons from deep traps, ~ 1.2 eV below the conduction band, and present in surprisingly large concentrations. From saturation photoconductive measurements¹⁰ in small test samples not involving domains, we found trap concentrations of about 10^{16} cm^{-3} , far exceeding the free-carrier concentration in the dark in our material.

(ii) Because the absorption coefficient in GaAs at

1.06 μm is small, $\approx 1-2 \text{ cm}^{-1}$ in our samples,¹¹ intense, focused radiation is required to obtain appreciable excitation. The domains, consisting of high-resistance regions about 1 mm wide, are particularly suited to detect such highly focused light because they concentrate most of the voltage drop across the sample.

The strong photoconductive response of acoustoelectric domains to a focused light beam provides a welcome new tool for scanning the spatial distribution and propagation of amplified acoustic flux. Conversely, a narrow propagating domain can be used to scan a light image projected on the surface of the sample. For either case the information is displayed very simply in the oscilloscope trace of the current pulse through the sample. These applications have been described elsewhere.¹²

In this paper we shall first summarize and then try to explain the various modulation effects produced by the intense light. The effects observed were very diverse, being strongly dependent on the stage of evolution of the acoustoelectric domain. We present here a simple model, based on small-signal acoustoelectric theory,^{13,14} which qualitatively explains the various effects simply in terms of the induced transient increase in electron concentration n . The latter affects the acoustoelectric amplification in two ways: (i) it changes the screening of the piezoelectric field and thus shifts the frequency dependence of the gain, an effect which played a major role in the initial recognition of the piezoelectric interaction¹⁵; and (ii) it changes the local carrier drift velocity in the domain and hence, the magnitude of the gain.

These two factors, acting sometimes coopera-

tively and at other times in opposition, determine the direction of the modulation of the acoustoelectric current and the acoustic flux, and can account for the diversity of the phenomena.

II. EXPERIMENTAL TECHNIQUE

All our measurements were done at 300 K with optically polished, *n*-type GaAs samples of average dimensions $2 \times 0.2 \times 0.1$ cm³, and oriented with their length along the $\langle 110 \rangle$ crystallographic axis. Typical electrical parameters were 6×10^{14} cm⁻³ carrier concentration and 0.6 (Ω cm)⁻¹ conductivity.

Propagating acoustic domains were generated in the usual fashion^{6,7} by the application of voltage pulses of 3–5- μ sec duration, with amplitudes in the range of 1–2 kV depending on the sample. The high-voltage pulses were supplied by a Velonex 360 generator at a repetition rate of 1 Hz to avoid excessive joule heating.

The optical setup is shown in Fig. 1. The source of high-intensity light for modulation of the acoustoelectric parameters in GaAs samples was a Q-switched YAlG: Nd laser (Quantronix Model 112A) which provided pulses of 200-nsec half-width at a peak power up to 3 kW. The intensity of light reaching the sample was controlled by a variable attenuator. Light emerging from the laser was polarized in a vertical plane by an intracavity polarizer P_1 . Two prism polarizers, P_2 and P_3 , external to the laser, were used to vary the light intensity between 0 and the full output, while maintaining an ultimate vertical polarization. The light intensity incident on the sample was proportional to $\cos^4 \alpha$, where α is the angle between the axis of the rotatable polarizer P_2 and the vertical axes of P_1 and P_3 . To monitor

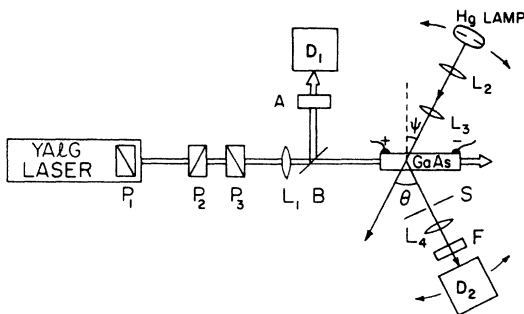


FIG. 1. Optical setup showing YAlG laser excitation of sample, and Brillouin scattering of light from Hg lamp. P_1 is an intracavity polarizer inside the YAlG: Nd laser, P_2 and P_3 are prism polarizers, L_1 – L_4 are lenses, B —beam splitter, A —light attenuator, S —aperture, F —interference filter. D_1 and D_2 are Si pin diode detectors. GaAs sample is illuminated in longitudinal geometry by the laser light (double line) of intensity monitored by D_1 , while the focused light of the Hg lamp (single line), scattered by angle θ , is detected by D_2 .

the intensity of light reaching the sample, a small fraction of it was deflected from the main beam by a beam splitter B , further attenuated at A (by another beam splitter and a light diffusing MgO surface), and detected by a Si photodiode detector D_1 . The lens L_1 was used to produce a spot of ≈ 1 mm diam in order to illuminate the whole domain.

The domains could be illuminated either in a transverse or a longitudinal geometry. In the former, the laser beam is incident perpendicular to the length of the sample and illuminates only a small segment of it, generally that through which the domain is passing. The timing of the light pulse has to be synchronized with the domain's passage through that segment. In the longitudinal case, the light beam passes through the whole length of the sample, filling the crystal with light, but with uniformity limited by an absorption coefficient¹¹ ≈ 1 –2 cm⁻¹. Proper timing of the light pulse allows illumination of the domain at any stage of its transit through the sample.

In addition to studying the photoconductive changes in current in the samples, we measured the concomitant changes produced in the phonon population in the domains. This was accomplished by Brillouin scattering measurements made just after the illumination of the domain by the YAlG laser pulse. For this purpose, a separate light source and detecting system were necessary. As shown in Fig. 1, a pulsed high-pressure Hg arc lamp was used as a source. By varying the angle of incidence ψ , of the Hg light on the sample as well as the observed scattering angle θ , we could study phonons of different frequencies, as has been described before.^{6,7} For on-axis phonons, the phonon frequency f is obtained from the scattering angle by the relation $f = (2v_s/\lambda) \sin(\frac{1}{2}\theta)$, where $\theta = 2\psi$, λ is the wavelength of light in the air, and v_s is the sound velocity. The intensity of light scattered at a given angle is a measure of the phonon intensity at the corresponding frequency.

Light from the mercury lamp was focused on the sample by two lenses L_2 and L_3 . This light, as a 10- μ sec pulse, was relatively long compared to the 0.2- μ sec laser pulse. The Brillouin scattered light was focused by a lens L_4 on a Si photodiode detector D_2 . An aperture S defined the collection cone. An interference filter F , passing light at 9800 ± 250 Å, was placed in front of the detector to prevent YAlG laser radiation from reaching the photodiode. The detector D_2 and its associated optical components were mounted on a rotatable arm, with the sample placed directly above the rotation axis. This permitted the variation of the scattering angle θ . Similarly, the incident angle ψ was changed by moving the arm containing the mercury lamp and its associated lenses about the

same axis.

Individual current and voltage pulses showing the effect of the laser modulation were generally displayed on a Tektronix 7623 storage oscilloscope. However, when we wanted to determine the variation of photocurrent (and/or Brillouin scattering signal) with incident laser intensity, we utilized two boxcar integrators. The YAlG light intensity, as monitored by the detector D_1 , was averaged by a PAR 162 Boxcar with 164 input plugin, using an 0.05- μ sec gate. The output was connected to the horizontal drive of an X-Y recorder. The photocurrent in the sample or the Brillouin scattering signal, depending on the measurement, was averaged by a PAR 160 Boxcar, also with an 0.05- μ sec gate, and its output was connected to the vertical axis of the recorder. Laser, mercury lamp, and high-voltage pulse, as well as the whole detection system, were triggered once per second from a common source.

III. EXPERIMENTAL RESULTS

A. Photoconductivity in domains

The photoconductive modulation by the laser light, at the different stages of development of the domain, is revealed directly in the current pulse shape. A summary of the dominant effects is presented in Figs. 2 and 3.

As an introduction, we show in Figs. 2(a) and

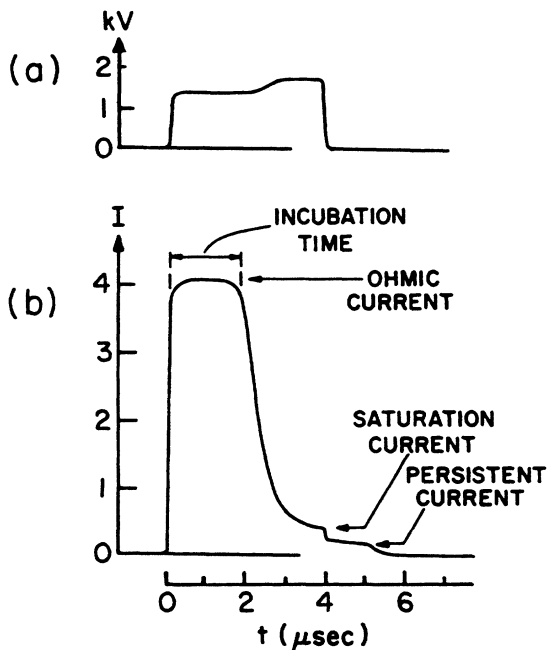


FIG. 2. (a) Voltage pulse and (b) current pulse characteristic of domain formation.

2(b) the voltage and current pulses in the dark to identify the stages of domain evolution. The external voltage applied to the sample is high enough to drive the electrons to a drift velocity v_d exceeding the appropriate phonon velocity v_s , which is the necessary condition for amplification. The circuit maintains a nearly constant voltage during each pulse. The current is initially constant at its ohmic value while the acoustic flux builds up from its thermal equilibrium value. After an incubation time of $\approx 2 \mu$ sec, the acoustic flux grows strong enough to cause the drop in current to a low saturation value. Generally, it is the acoustic flux near the cathode that is most favorably amplified and eventually forms a domain, about 1–2 mm wide, which propagates through the sample with velocity v_s . The drop in current is caused by strong stimulated emission of phonons by the electrons, due to the amplified phonons in the domain. The domain becomes a region of very high resistance which concentrates most of the voltage drop across the sample. After the external voltage pulse is shut off at $t \approx 4 \mu$ sec, the current persists for about a microsecond as the energy and momentum concentrated in the acoustic flux are transferred back to the electrons.^{16,17}

Next we shall demonstrate the diverse ways in which the current trace is affected by the YAlG laser pulse. In Figs. 3(a) and 3(b), voltage and current pulses in the dark are drawn again with solid lines. The superimposed current spikes indicated by dashed lines are caused by light pulses incident in the transverse illumination geometry. The four current spikes shown at t_1 – t_4 are representative of the four characteristic stages in domain evolution. If the light pulse illuminates the fully grown domain at time t_2 , then the current is increased by as much as an order of magnitude at

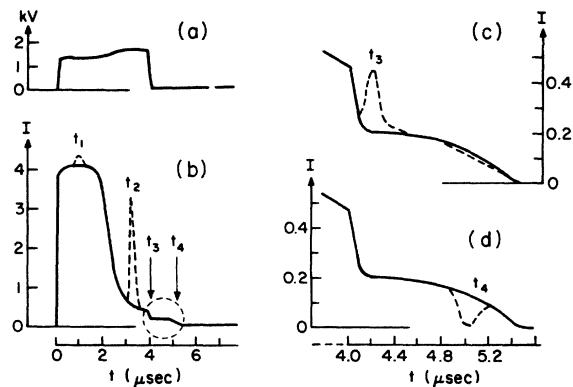


FIG. 3. (a) Voltage pulse and (b) current pulse with superimposed photoconductive spikes (dashed lines) produced by the laser light pulses in transverse geometry. The circled area is shown enlarged in (c) and (d).

the peak of the light pulse. However if the same spot is illuminated at any earlier time t_1 , either before the domain has formed, or before it reaches the spot, the photoconductive spike is very weak or completely suppressed. The persistent current regime is contained in the circled part of the current trace in Fig. 3(b), and shown enlarged in 3(c) and 3(d). When the domain is illuminated at time t_3 , just after the external voltage is shut off and while the acoustic intensity is still very strong, then the current is increased by the light pulse. However if we wait till t_4 , after the persistent current and hence the acoustic flux has significantly attenuated, we find that the current is now strongly reduced by the light pulse. It must be emphasized that at times t_2 , t_3 , and t_4 no perceptible effect was observed if light passed through the sample outside the domain.

In general, the timing and duration of the current modulation pulse correspond closely to that of the light pulse. However there are some interesting cases of after effects which will be discussed later.

B. Comparison of photocurrent and Brillouin scattering data and preliminary analysis

To supplement the phenomena illustrated in Fig. 3, a series of measurements of current modulation versus incident light intensity was taken. In addition, Brillouin scattering measurements were made in the domain to determine the influence of the intense light on the growth of the acoustic flux. For greatest convenience, the intense YAIG light was applied here in the longitudinal geometry, as shown in Fig. 1. The combination of the photoconductive and acoustical-phonon measurements was extremely useful for elucidating the details of the photoacoustoelectric effect.

In Fig. 4, the photoexcitation current measured at its peak pulse value is plotted against the incident light intensity in the t_1 and t_2 regimes. In the former, the current grows monotonically with the light intensity, achieving a 75% enhancement over the dark value. In contrast, in the t_2 regime the increase in current is much greater, up to a value over seven times the dark current. Since the domain region concentrates about 90% of the sample's resistance, the creation of extra free carriers in this region greatly increases the current in the sample. Auxiliary electrical probe measurements showed that the electric field across the domain was partially shorted out by the light pulse.

The very weak effect of light at t_1 in the Ohmic regime is due to the fact that the intense illumination affects only a relatively small segment of the

sample, and hence modulates only a small fraction of the total resistance. This is most obvious in transverse illumination geometry, but is still a factor in longitudinal illumination because of the appreciable absorption of light along the length of the sample. That the local conductivity modulation is actually much higher than is apparent from the gross current changes, was verified by estimates based on the fractional volume of the sample illuminated, and by supplementary experiments (described in Sec. III C) on small samples which could be completely and uniformly filled with light. From the fact that there is indeed a large conductivity increase in the Ohmic regime, we can conclude that there must be a large increase in free-carrier concentration.

Returning to the t_2 regime, we note that as a consequence of the increase in excess free carriers cited above, there must be a modulation of the strength of the acoustoelectric interaction. Estimation of the direction of this effect requires the detailed theoretical analysis presented in Sec. IV. However, some immediate insight is obtainable from the Brillouin scattering experiments which tell us how the phonon population is changed by the light pulses. The scattering measurements were made 250 nsec after the peak of the YAIG light pulse. The mercury-lamp intensity is much less than the YAIG laser intensity and contributes negligibly to the photoconductive effects. The

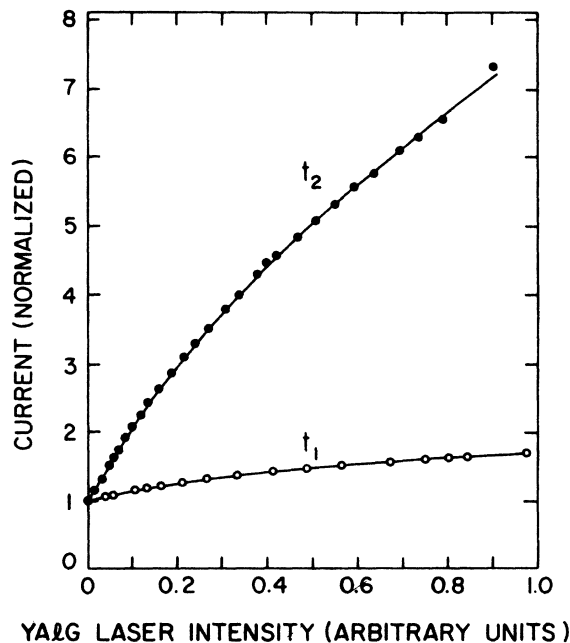


FIG. 4. Variation of current with YAIG laser intensity in longitudinal geometry. The top curve was taken in the t_2 regime, the bottom curve in the t_1 regime.

Brillouin scattering curves, taken in the t_2 regime for phonons of frequencies equal to 0.8 and 2.3 GHz, are shown in Fig. 5. We see that the phonon intensity is considerably increased by the YAlG laser excitation, by as much as 40 and 80% respectively at the two frequencies. From this we can conclude that the acoustoelectric gain was transiently increased.

To analyze the last result, we have to examine what factors determine the acoustoelectric gain. For simplicity, we consider only the small-signal form¹⁴ of the gain, which can be written as $\alpha = \alpha_0 \gamma$, where $\gamma = v_d/v_s - 1$ and the coefficient α_0 is given by the expression²⁻⁷

$$\alpha_0 = K^2 \omega_D (\omega/\omega_m + \omega_m/\omega)^{-2}. \quad (1)$$

K , the electromechanical coupling constant, is proportional to the piezoelectric tensor; $\omega_m = (\omega_D \omega_C)^{1/2}$, where $\omega_D = ev_s^2/\mu kT$ is the diffusion frequency, and $\omega_C = \sigma/\epsilon$ is the dielectric relaxation frequency; e , μ , k , T , σ , and ϵ are, respectively, the electron charge, electron mobility, Boltzmann constant, temperature, conductivity,

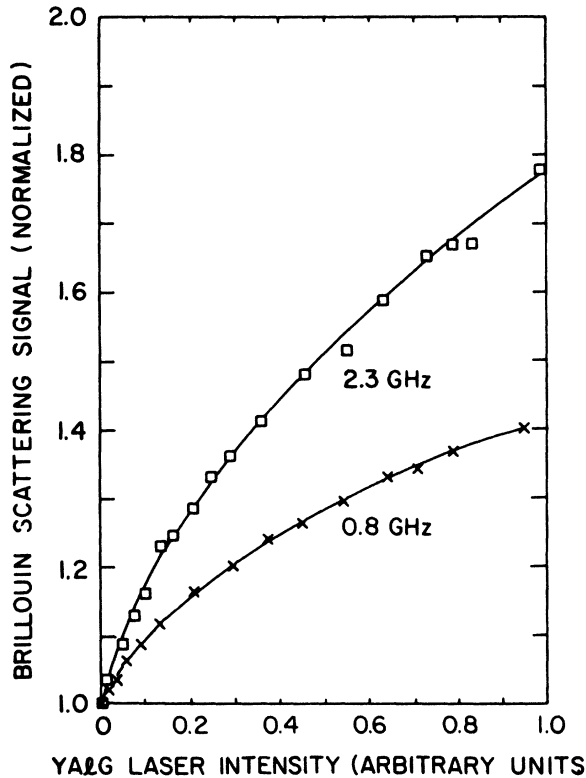


FIG. 5. Dependence of Brillouin scattering intensity of light from the Hg lamp on YAlG laser intensity. The laser pulse preceded the Brillouin scattering measurement by 250 nsec. Both curves were taken in the t_2 regime. The upper one is for scattering by 2.3-GHz phonons, the lower one for 0.8-GHz phonons.

and dielectric constant. The expression in Eq. (1) is valid if (a) $ql < 1$, where q is the phonon wave vector and l is the mean free path of electrons; and if (b) $\gamma \ll (\omega_C/\omega + \omega/\omega_D)$. These approximations apply reasonably well to our material.

The acoustoelectric gain is maximum for the phonons with the angular frequency $\omega = \omega_m$. Since $\sigma = ne\mu$, the frequency of the maximum acoustoelectric gain $f_m = \omega_m/2\pi$, is proportional to \sqrt{n} . In Fig. 6, α_0 is plotted as a function of the acoustic frequency f , for $n_0 = 6 \times 10^{14} \text{ cm}^{-3}$ and also for $4n_0$ and $10n_0$. The increase in n modifies ω_C and hence the screening of the piezoelectric field. This simply shifts the acoustoelectric gain curve $\alpha_0(f)$ to higher frequencies, decreasing the gain coefficient at the frequencies $f \approx f_m$, which correspond to the data of Fig. 5.

In spite of the expected reduction of α_0 by the illumination, we found in Fig. 5 that the phonon intensity was increased. Apparently the gain has increased, indicating that the factor γ , must have increased more than enough to compensate for the decrease in α_0 . It follows then, that with increasing light intensity, v_d must increase in the domain along with n , and that the current density $j = nev_d$ must therefore increase faster than n . Thus, the high-resistance domain shows a faster than linear response to carrier excitation.

In Fig. 7 we present the photoconductive and Brillouin scattering curves at t_3 , just after the voltage pulse is shut off, when a persistent current is driven by the still very strong acoustic flux. The current increases with light intensity until it is about twice the value in the dark, then starts to decrease. The Brillouin scattering curve shows a decrease of phonon intensity at 0.8 GHz. What happens here can be explained as follows: In

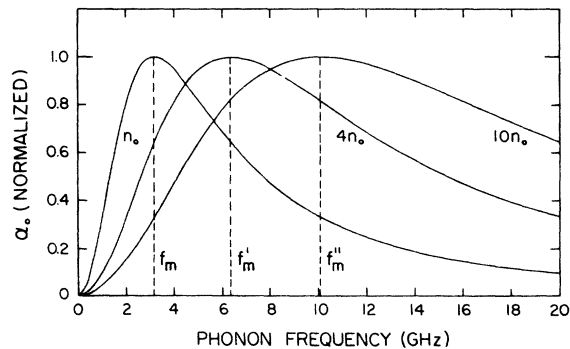


FIG. 6. Piezoelectric coupling coefficient α_0 , calculated from Eq. (1), as a function of acoustic frequency, for three values of the carrier concentration: $n_0 = 6 \times 10^{14} \text{ cm}^{-3}$, $4n_0$, and $10n_0$. Frequencies of maximum acoustic gain for these three cases are represented by f_m , f'_m , and f''_m , respectively.

the t_3 regime, the persistent current density is saturated at approximately $j_p = n_0 e v_s$ as the acoustic flux drives nearly all the electrons at a drift velocity very close to v_s .^{7,17} If the light pulse increases the number of electrons from n_0 to n , it causes an enhancement of the persistent current. It should be noted here, that had there been an increase in holes, they would have been dragged by the phonons in the same direction as the electrons and a persistent current in the opposite direction would have been produced, thus giving a net decrease in persistent current. The fact that a sharp increase in j_p is observed, means that production of electrons by the laser light is strongly predominant over production of holes.

As the amplified phonon flux is forced now to drive more electrons, it must attenuate faster. In confirmation of this expectation of enhanced acoustoelectric attenuation, the Brillouin scattering data at 0.8 GHz show more than 35% decrease of the phonon intensity after application of the light pulses. The current pulse trace in the insert of Fig. 7 shows indirectly the weakening of the total acoustic flux. This is revealed by the fact that after the light pulse is over, the persistent acoustoelectric current drops to a value which is below the original dark current level.

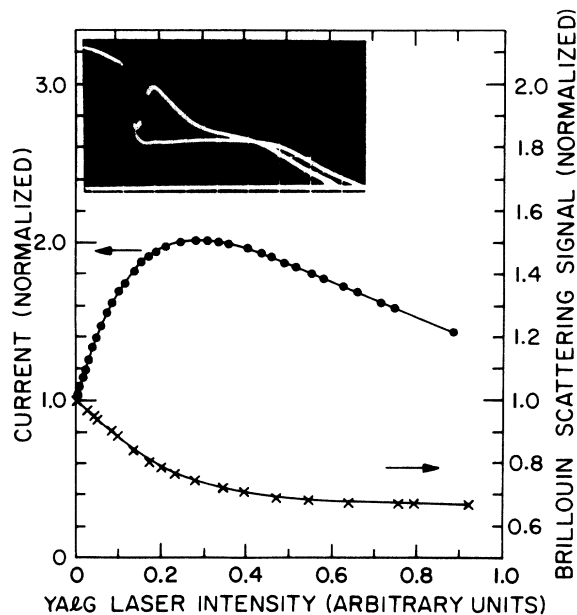


FIG. 7. Current and Brillouin scattering curves in the t_3 regime, as a function of the peak laser light intensity in longitudinal geometry. The scattering curve is for 0.8-GHz phonons. Photograph in the insert shows two persistent current traces, one in the dark, another with the laser pulse illumination of the intensity chosen to maximize the current increase. Note also that after illumination the current decays faster.

In the t_4 regime, the acoustic flux has attenuated substantially, and therefore, the persistent current has decreased below its saturation value.

Fig. 8 shows that, with increasing light intensity, the persistent current at this stage drops rapidly, until it is almost completely quenched at the full laser power. Correspondingly, the density of 0.8-GHz phonons is significantly enhanced at high light intensity. The fact that j_p is forced to decrease means that there is a reduced rate of momentum transfer from the phonons to the electrons. This is consistent with the observation that the acoustic flux at frequencies $f < 1.5$ GHz does not attenuate as fast as in the dark.

The analysis of why j_p decreases at increased light intensity, in spite of the higher carrier concentration, is rather involved as various competing factors have to be taken into account. The dependence of j_p on changes in α_0 and γ , on the acoustic flux spectrum, on circuit conditions, and illumination geometry is considered in detail in Sec. IV.

C. Photoexcitation mechanism

The photoconductive effects observed in the four stages of acoustic domain evolution, all required an increased carrier concentration for their explanation. Furthermore, the results in the per-

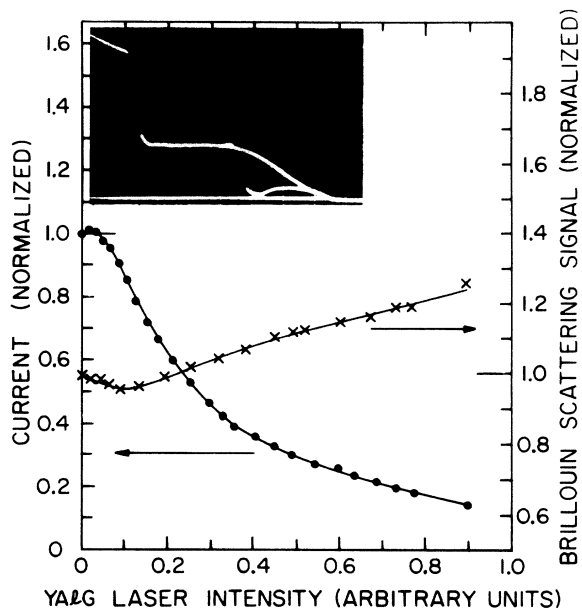


FIG. 8. Current and Brillouin scattering curves in the t_4 regime, as a function of the peak laser light intensity in longitudinal geometry. The scattering curve is for 0.8-GHz phonons. Photograph in the insert shows two persistent current traces, one in the dark, another with the laser pulse of the maximum intensity available.

sistent current regime at t_3 required a dominance of electron concentration. When these effects were first observed, it was difficult to understand how the YAlG laser light could produce a very large increase in electron concentration, especially in view of the relatively weak absorption (less than 2 cm^{-1}) in this material. To ascertain the magnitude of the photoconductive effect without the complication of domains, we measured the effect in the Ohmic regime. To get meaningful data it was necessary to produce uniform excitation in the whole sample volume between the electrical contacts. The samples used for the acoustic amplification could not be utilized in this experiment because of their large dimensions. In these samples, in the transverse geometry, only a small segment is affected by light. In the longitudinal geometry, the light beam excites carriers throughout the sample but not uniformly. For samples 2 cm long, an absorption coefficient of only 1.5 cm^{-1} causes the light intensity to drop along the sample to a level of $\approx 5\%$ of its initial value. To attain uniform light intensity, small samples $0.2 \times 0.2 \times 0.05 \text{ cm}^3$ had to be used, with light uniformly incident on the large side.

The increase of conductivity with light intensity was found to be sublinear in the whole range studied, ultimately approaching a saturation level¹⁰ at intensities of $\approx 4 \text{ MW/cm}^2$. This high intensity, providing a 25-fold enhancement in conductivity, was obtained with a more powerful laser¹⁸ than the one we used for modulation of acoustoelectric instabilities. However, even the weaker laser light provided a 4–10 times increase in conductivity, depending on the sample used. The peak light intensity in the experiments described in this paper was $\approx 70 \text{ kW/cm}^2$. After reflection and attenuation losses, it produced a fourfold increase in the local carrier concentration.

The only mechanism that can account for very strong photoenhancement of the conductivity and its ultimate saturation is the excitation of electrons from deep traps, present in concentrations $\approx 10^{16} \text{ cm}^{-3}$. A more detailed account of the ultrahigh intensity measurements and the prevalence of such deep traps at $\approx 1.2 \text{ eV}$ below the conduction band in GaAs has been published elsewhere.¹⁰ As discussed there, any major contribution from nonlinear optical effects, hot carrier effects, or generation of holes was ruled out.

IV. THEORETICAL ANALYSIS OF MODULATION OF ACOUSTOELECTRIC INTERACTIONS

A. Model and basic equations

We shall now discuss in detail the modulation of acoustoelectric current and acoustic flux by a

photoexcited excess electron population in n -GaAs. We use a simple model²⁻⁷ based on small-signal acoustoelectric theory, which neglects any nonlinear phonon-phonon interactions, or possible dependence of the piezoelectric interaction strength on acoustic intensity, and other strong flux effects. Nevertheless this very simplified approach suffices to explain qualitatively all the aspects of the observed phenomena.

The rate of change of momentum for an interacting system of electrons and acoustic waves in the presence of a driving electric field is given by^{2,6,7}

$$neE_d = \frac{nev_d}{\mu} + \left(\frac{v_d}{v_s} - 1 \right) \sum_f \frac{\alpha_0 \phi}{v_s}. \quad (2)$$

E_d represents the average electric field in a region much larger than an acoustic wavelength, but small compared to the spatial distribution of the acoustic flux. ϕ is the acoustic energy density for phonons and is a function of frequency f . The first term on the right-hand side is the rate of momentum loss for electrons via Ohmic processes while the second term describes the acoustoelectric rate of momentum transfer to the acoustic flux, summed over all frequencies.

The phonon amplification (or attenuation) rate depends on the acoustoelectric gain coefficient $\alpha_0 \gamma$, through the relation^{2,6}

$$\frac{d\phi}{dt} = \alpha_0 \gamma \phi - \alpha_L \phi + (\alpha_0 + \alpha_L) \phi_0, \quad (3)$$

where the term $\alpha_L \phi$ describes the nonelectronic or lattice attenuation at a given acoustic frequency. The last term permits $d\phi/dt$ to go to zero at $v_d = 0$ and $\phi = \phi_0$, where ϕ_0 is the thermal equilibrium acoustic energy density.

Starting from these two coupled equations, we can determine what happens to the current and acoustic flux when the electron concentration n is suddenly increased by a laser pulse. We expect that α_0 will adjust to a new value within a few electron collision times. The acoustic flux takes much more time to change as n is increased. Its growth rate in Eq. (3) changes through its dependence on α_0 and also through the dependence of γ on n , the latter being determined from the solution of Eq. (2). We neglect any change in electron mobility associated with the excitation of the excess carriers, either due to the change in the charge status of deep traps¹⁹ or due to carrier heating by the laser light. The very large increase in conductivity justifies the assumption that the increase in n is the overwhelmingly dominant effect. Finally, an estimate of the energy dissipated in the sample by a single light pulse showed that the change in sample temperature is less than 1°K .

In solving Eq. (2) for the dependence of γ on n , we impose the experimental condition that the total voltage across the sample is maintained constant, either at the voltage V produced by the external pulse, or at zero after the pulse is shut off. The acoustic flux is taken to be confined in a narrow propagating domain of width $d \ll L$, where L is the length of the sample. For the illumination geometry, we consider two simple cases: (a) transverse geometry, where the laser pulse uniformly illuminates only the domain region while the rest of the sample is kept dark, and (b) an idealized longitudinal geometry, where n is uniformly increased throughout the sample, a condition that is not attained experimentally. Its analysis is included to see how illumination geometry can affect the observations.

The experimental data in Figs. 3 and 9 were taken in the transverse geometry, and the rest with the light beam passing through the length of the crystal. However, because of absorption, even the latter situation falls closer to the transverse than to the idealized longitudinal case.²⁰

1. Case (a): Transverse geometry

The carrier concentration and drift velocity are taken to be n_0 and $(v_d)_0$ in the dark part of the sample and n and v_d in the illuminated segment. We assume the current continuity relation is applicable even when a strong domain is present. Then

$$n_0(v_d)_0 = nv_d. \quad (4)$$

Using Eqs. (2) and (4), and integrating over the

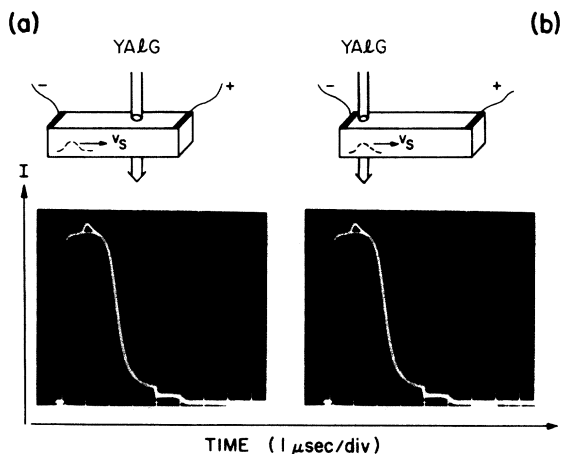


FIG. 9. Current modulation effects for light incident on the sample in the t_1 regime in transverse geometry. (a) Position of the light beam does not coincide with the location of the embryonic domain. Only a small current spike is observed. (b) Light beam illuminates the embryonic domain. In addition to the current spike, there is an increase in the incubation time of the domain.

dark and illuminated segments of the sample, we obtain for the total voltage across the sample

$$V = \frac{n}{n_0} \frac{v_d}{\mu} L + \frac{\bar{\alpha}_0(v_d/v_s - 1)\Phi}{Anev_s}, \quad (5)$$

where Φ , the total acoustic energy in the domain, and $\bar{\alpha}_0$, an effective average acoustoelectric interaction coefficient, are defined by

$$\bar{\alpha}_0\Phi = A \int_0^L \sum_f \alpha_0\phi dx, \quad (6)$$

where A is the cross sectional area of the sample. Even though the integration is over the total length of the sample, the only significant contribution comes from the domain region. From Eq. (5), an expression for the electron drift velocity in the domain is obtained

$$\frac{v_d}{v_s} = \frac{(n_0/n)(v_i/v_s) + \bar{\alpha}_0\Phi C(n_0/n)^2}{1 + \bar{\alpha}_0\Phi C(n_0/n)^2}, \quad (7)$$

where $v_i = \mu V/L$ is the initial Ohmic drift velocity of the electrons in the absence of the acoustic flux; generally $v_i/v_s \approx 20$ in our experiments. C is a constant, equal to $\mu/(n_0ev_s^2LA)$.

2. Case (b): Longitudinal geometry

For the case where the whole sample is uniformly illuminated, n and v_d are also uniform in the entire sample, and integration of Eq. (2) gives

$$\frac{v_d}{v_s} = \frac{v_i/v_s + \bar{\alpha}_0\Phi C(n_0/n)}{1 + \bar{\alpha}_0\Phi C(n_0/n)}. \quad (8)$$

Using Eq. (3) describing the rate of change of the acoustic energy density in conjunction with either Eq. (7) or (8), we can determine the modulation of the current and acoustic flux by the light at the different stages of the domain evolution.

B. t_1 regime

In the t_1 regime the acoustic flux is still very weak, and hence,

$$\bar{\alpha}_0\Phi C \ll 1. \quad (9)$$

The effect of the light pulse in transverse geometry is to multiply the left-hand side of this relation by $(n_0/n)^2$, making it still smaller. With this condition, Eq. (7) reduces to $v_d = (n_0/n)v_i$. Locally, n may be increased severalfold but the current is changed only slightly since only about $\frac{1}{20}$ of the sample is illuminated. The local reduction of gain coefficient γ can cause, for a light pulse of sufficient intensity, a crossover from net amplification ($\alpha_0\gamma > \alpha_L$) to net attenuation ($\alpha_0\gamma < \alpha_L$). In addition, the $\alpha_0(f)$ curve is shifted to higher frequencies, permitting this crossover to occur at lower light

intensities for most of the frequencies of interest. If the laser beam is focused on a spot near the negative end of the sample, through which an embryonic or not-yet-developed domain is passing, the reduction in net gain described above can cause an appreciable increase in the incubation time of the domain. This is demonstrated in Fig. 9(b). By contrast, if the laser light is incident at any other spot along the sample, it produces only the small spike in the current trace shown in Fig. 9(a). The increase in the incubation time corresponds well to the width of the intense light pulse, and is sensitive to synchronization of the laser pulse with the embryonic domain. This result provides a simple means of locating where the domain originates, since we can now "see" it at an early stage, before it can affect the sample's resistance.

In the longitudinal case, Eq. (8) shows v_d , and hence, γ to be independent of light intensity. However, an increase in the incubation time in this case can be caused by a decrease in $\bar{\alpha}_0$ as the α_0 curve is transiently shifted to higher frequencies.

C. t_2 regime

In the t_2 regime, the acoustic flux is very strong and practically all the voltage drop occurs across the domain. For $n = n_0$, the current density drops to a level which is found to saturate with increasing applied voltage. We can express this by $j_{\text{sat}} \equiv n_0 e (v_d)_{\text{sat}}$, which is about 10% of its original Ohmic value. This situation corresponds to the condition

$$\bar{\alpha}_0 \Phi C \gg 1. \quad (10)$$

Here the saturation drift velocity in the dark is given by

$$\frac{(v_d)_{\text{sat}}}{v_s} = 1 + \frac{v_i/v_s}{\bar{\alpha}_0 \Phi C}. \quad (11)$$

Measurements (Fig. 3) show that the saturation current density j_{sat} is close to $2n_0 e v_s$, which implies that $\bar{\alpha}_0 \Phi C$ is close to v_i/v_s . However, in such strong acoustic flux, α_0 is not necessarily given by the small-signal relation, Eq. (1), and the flux distribution Φ has been influenced by nonlinear phonon-phonon interactions.^{6,7}

When the light pulse is applied, for sufficiently strong flux we have the condition

$$(n_0/n)^p \bar{\alpha}_0 \Phi C \gg 1, \quad (12)$$

where $p = 1$ or 2 for longitudinal and transverse geometry, respectively. Under this condition

$$\frac{v_d}{v_s} = 1 + \frac{(n/n_0)(v_i/v_s)}{\bar{\alpha}_0 \Phi C}, \quad (13)$$

the same for both geometries.

We can now explain the very rapid increase of current with light intensity in the t_2 regime. From Eq. (13), we see that v_d should initially increase linearly with n , and the current density $j = n e v_d$ should grow faster than n .

For large n , we must use the full expressions of Eqs. (7) and (8). The resulting dependence of j on n is plotted in Fig. 10 for a few values of the parameter $D = \bar{\alpha}_0 \Phi C$. The increase of j with n in this case is faster for the idealized longitudinal geometry. In comparing Fig. 10 with experiment, it should be remembered that n increases sublinearly with light intensity, making the variation of j with light intensity slower than its variation with n . On the other hand, we note that as n increases, α_0 and hence D , decrease for the frequencies $f \lesssim f_m$ corresponding to most of the acoustic flux. Thus j must increase more rapidly than would appear from the fixed D curves in Fig. 10.

As a point of reference for comparing the theoretical curves with experiment (Fig. 4) the maximum value of n achieved in the domain is $\approx 4n_0$. The experimentally observed, sevenfold increase in j agrees reasonably well with the calculated curves in Fig. 10 for $n = 4n_0$ and $D = 20$, especially when we consider that the experimental situation was intermediate between the two ideal geometries.

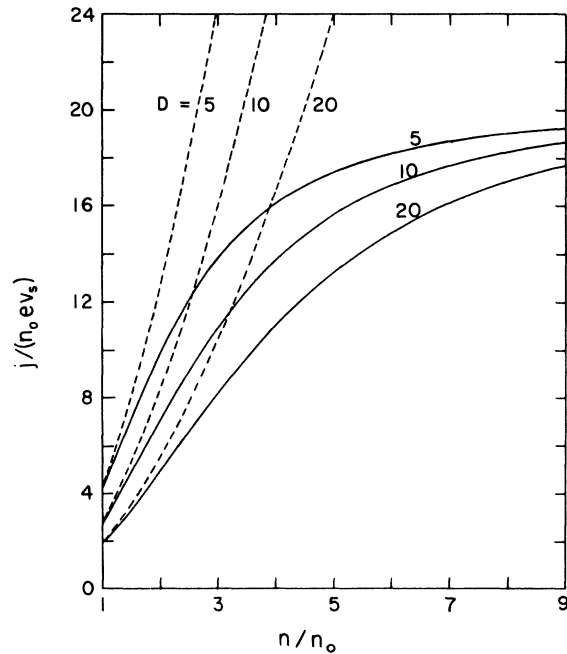


FIG. 10. Normalized current density in the t_2 regime as a function of the carrier concentration, calculated for several values of the parameter D . Solid lines represent the ideal transverse case, dashed lines the ideal longitudinal geometry.

Next we discuss the data of Fig. 5, which shows the enhancement of the acoustic flux by the light pulse. From Eq. (3), the flux growth rate is determined by the acoustoelectric gain $\alpha_0\gamma$. As illustrated in Fig. 6, α_0 is expected to decrease at frequencies $f \lesssim f_m$, and to increase only at $f \gg f_m$. The calculated variation of the factor γ with n , which applied to all frequencies, is shown in Fig. 11. For both longitudinal and transverse geometries γ increases with n , but the increase is faster and monotonic for the former case. Effectively, γ increases faster than is shown if we take into account the fact that D decreases as n increases. Thus the net acoustoelectric gain depends on the balance between various factors and also on the frequency of the phonons. Since the fractional decrease in α_0 is less at 2.3 GHz than at 0.8 GHz we can understand greater enhancement of the flux at the higher frequency. For this frequency, the data of Figs. 6 and 11 show that for $n = 4n_0$ in the domain, the increase in γ can more than compensate for the decrease in α_0 , which explains the enhanced flux growth. For the lower frequency, the enhancement of the acoustoelectric gain seems rather marginal. However, at the low frequencies the contribution to the growth from nonlinear down conversion from flux at higher frequencies may well outweigh that from acoustoelectric gain. The theoretical curves predict that at $n \gg 4n_0$ the acoustoelectric gain would be reduced.

The observed flux increase in the domain clearly demonstrates that γ must have been increased, since α_0 must have decreased at the measured frequencies. An increase in γ is consistent with defining γ as $v_d/v_s - 1$. We may consider what would happen if we had chosen an alternative definition²¹ of γ as $\mu E_d/v_s - 1$, where E_d is the local field in the domain. Our probe measurements of this field showed it to be appreciably decreased

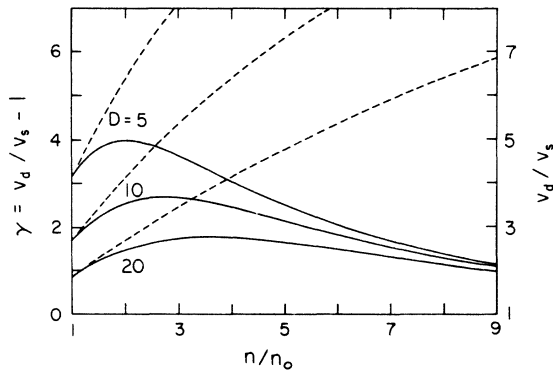


FIG. 11. Gain coefficient γ and v_d/v_s in the t_2 regime as a function of n , calculated for several values of D . Solid lines represent the ideal transverse geometry, dashed lines the ideal longitudinal geometry.

when the domain is strongly illuminated. Thus the alternative definition would have given a decrease in γ and it would not have been possible to explain the increase in flux. The light modulation experiment therefore indicates that the latter form of γ is not tenable.

D. t_3 and t_4 regimes

When the voltage across the sample is cut off, we obtain a persistent current j_p given by

$$\frac{j_p}{n_0 e v_s} = \frac{n v_d}{n_0 v_s} = \frac{\bar{\alpha}_0 \Phi C (n_0/n)^{p-1}}{1 + \bar{\alpha}_0 \Phi C (n_0/n)^p}. \quad (14)$$

We consider first the condition $n = n_0$. If the voltage drops to zero very rapidly, the acoustic flux is initially as strong as in the t_2 regime; hence Eq. (14) simplifies to give $v_d \approx v_s$. (Actually, $v_d/v_s = 0.95$ for $D = 20$ and $n = n_0$). The persistent current $j_p = n e v_d$ is proportional to the carrier concentration, as long as $v_d \approx v_s$. However for a sufficiently large increase in n , v_d is reduced according to Eq. (14). Calculations of v_d/v_s , γ , and j_p as a function of n are plotted in Figs. 12 and 13. The calculations show that v_d decreases with increasing n for both illumination geometries, and the persistent current which was enhanced by weak light, continues to increase (but tends eventually to saturate) with n for $p = 1$ (longitudinal case) or passes through a maximum as the light intensity is increased for $p = 2$ (transverse case). The experimental curve of Fig. 7 showed an initial increase in j_p with n , in agreement with the theory. As n is increased further, j_p reaches a peak and then decreases. This can be understood from the transverse geometry case in Fig. 13 if we invoke the decrease in $\bar{\alpha}_0$, hence D , with increasing n .

The initial increase of j_p with n depended on the condition that the flux was very strong, corresponding to Eq. (10). For weaker flux (smaller D)

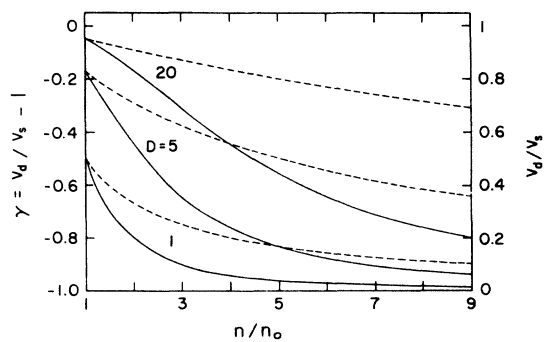


FIG. 12. Gain coefficient γ and v_d/v_s in the t_3 and t_4 regimes as a function of n , calculated for several values of D . Solid lines represent the ideal transverse geometry, dashed lines the ideal longitudinal geometry.

and/or large n/n_0 , quite different results are obtained. As the acoustic flux attenuates in going from the t_3 to the t_4 regime, the calculated curves of Figs. 12 and 13 for progressively smaller values of D become applicable. The weak flux curves of j_p in Fig. 13 for $D=5$ and $D=1$ in transverse geometry show very small, if any, initial positive increment before going negative with increasing n . This result is in good agreement with the experimental data for j_p in Fig. 8. However, the strong dependence of the theoretical results in Fig. 13 on the illumination geometry should be noted. Our experimentally observed decrease in j_p with n requires a dominantly transverse geometry in which the excess electrons are produced mainly in the domain.

Figure 13 and Eq. (12) indicate that it is the ratio of the $\bar{\alpha}_0 \Phi C$ term to n/n_0 which should determine the direction of the change in the persistent current during illumination. This is demonstrated nicely by the experimental curve of Fig. 14, where the decay of the persistent current is shown for several different light intensities. The measurement was done by slowly scanning the triggering time of the consecutive laser pulses through the entire persistent current region. A boxcar gate moving at the same rate provided a record of the magnitude of the current at the peak value of the

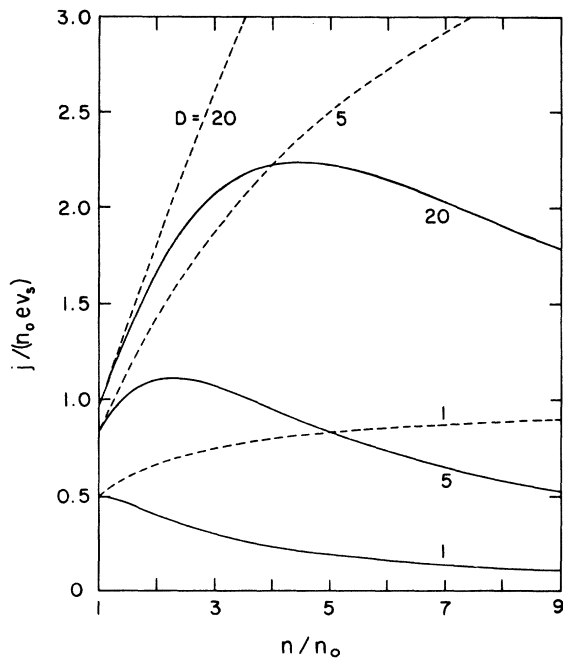


FIG. 13. Normalized current density in the t_3 and t_4 regimes as a function of the carrier concentration, calculated for several values of the parameter D . Solid lines represent the ideal transverse geometry, dashed lines the ideal longitudinal geometry.

light pulse. The change over from positive to negative current modulation is readily seen to occur at an earlier time (i.e., at stronger acoustic flux) for more intense light.

Finally, we turn to the modulation of the acoustoelectric attenuation in the persistent current regime. The persistent current is a manifestation of the rate of loss of momentum from the acoustic flux to the carriers. Thus, the change of j_p with light provides a measure of the change of the acoustoelectric attenuation of the integrated flux Φ . From Eq. (3), the rate of change of the total acoustic momentum in the domain Φ/v_s , through electronic losses alone is given by

$$\left(\frac{d(\Phi/v_s)}{dt}\right)_{e1} = \bar{\alpha}_0 \gamma \left(\frac{\Phi}{v_s}\right). \quad (15)$$

Then, using Eq. (5) with $V=0$, we can express $(d\Phi/dt)_{e1}$ in terms of the persistent current j_p and carrier concentration n in the domain. For transverse geometry,

$$\left(\frac{d\Phi}{dt}\right)_{e1} = -\left(\frac{n}{n_0}\right) j_p v_s \frac{LA}{\mu}, \quad (16)$$

while for longitudinal geometry, the factor n/n_0 is replaced by unity. Thus from the variation of nj_p or j_p with light intensity, depending on the geometry, we should be able to predict how the acoustic

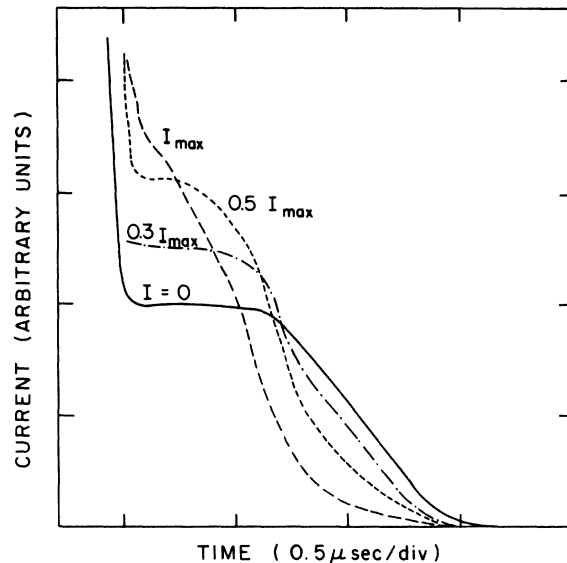


FIG. 14. Experimental curves of the decay of the persistent current j_p at different peak light intensities. The solid line represents j_p in the dark ($I=0$), the dashed lines are for three illumination intensities. The measurement was done by slowly scanning the firing time of the consecutive laser pulses. A boxcar gate, moving at the same rate, provided a record of the magnitude of the current at the peak value of the light pulses as a function of time.

attenuation changes.

In the t_3 regime, the initial rapid increase in j_p and n at low light intensities enhances the attenuation rate and explains directly the induced decrease in phonon intensity (enhanced attenuation) seen by Brillouin scattering in Fig. 7. At higher light intensity, j_p reaches a peak and decreases, while n continues to increase sublinearly. The opposing influences of these two factors are reflected in the data in Fig. 7, which show that the acoustic flux stops decreasing and becomes nearly constant.

The t_4 regime is an extension of this situation and applies to weaker flux, consisting of the most slowly decaying low-frequency components. The fast drop in persistent current with light intensity (Fig. 8) is the dominant factor in accounting for the observed decrease in acoustoelectric attenuation. The latter is manifested by a residual acoustic flux signal whose magnitude increases with light intensity.

So far we have described the change in acoustic attenuation of the integrated flux and assumed it to apply to the flux at 0.8 GHz. This assumption is reasonable since the frequencies $f \ll f_m$ are strongly dominant⁷ after prolonged attenuation. However, if we wish to discuss the attenuation of any particular frequency component we still have to determine its dependence on $\alpha_0\gamma$. Our theoretical curves in Fig. 12 show that the coefficient γ becomes more negative during the light pulse, which serves to increase the acoustoelectric attenuation at all frequencies. The observed reduction of attenuation of 0.8-GHz flux indicates that α_0 decreases more than enough to compensate for the opposing trend of γ . However, at the higher frequency, $f = 2.3$ GHz, we did find increased attenuation. Here, as could be expected, the decrease in α_0 was not large enough to compensate for the change in γ . In this case, just as in the t_2 regime,

we find that the acoustoelectric attenuation is determined by opposing tendencies in α_0 and γ , with the outcome dependent on the acoustic frequency.

V. CONCLUSIONS

We have described a series of measurements involving transient photoconductive modulation of acoustoelectric current and of acoustic flux in propagating domains of amplified phonons. It was determined that the primary effect of the light pulse is to produce a large number of excess free electrons by photoexcitation from deep traps. A model based on small-signal acoustoelectric theory, was used to explain qualitatively how the pulse change of carrier concentration produced the diverse modulation effects seen at different stages of domain development. For our limited purposes it was not necessary to take into account nonlinear interactions between very strongly amplified phonons, which are known to influence greatly the form of the amplified phonon spectrum.^{6,7}

The analysis showed how the change in gain coefficient $\gamma = v_d/v_s - 1$ and the piezoelectric coupling coefficient α_0 affected the rate of growth or decay of acoustic phonons and their spectral distribution. The increase of the incubation time, if the light beam illuminated the position of the embryonic domain, gave us information about very early domain development, before it showed up in the resistance of the sample. The evidence of enhanced gain in the domain in the t_2 regime strongly favors the view that v_d rather than μE is the dominant factor in determining the coefficient γ . The dependence on acoustic frequency of the amplification in the t_2 regime and of the attenuation modulation in the t_4 regime, demonstrated the transient shift of the α_0 curve to higher frequencies by the sudden increase in electron concentration.

†Work supported by NSF Grant No. GH 43409 and by MRL Program No. DMR 72 03018A03.

*Formerly J. K. Wajda.

¹P. O. Sliva and R. Bray, Phys. Rev. Lett. **14**, 372 (1965).

²R. Bray, IBM J. Res. Dev. **13**, 487 (1969).

³N. I. Meyer and M. H. Jorgensen, Festkörperprobleme **10**, 21 (1970).

⁴M. B. N. Butler, Rep. Prog. Phys. **37** 421 (1974).

⁵H. Kuzmany, Phys. Status Solidi A **25**, 9 (1974).

⁶D. L. Spears, Phys. Rev. B **2**, 1931 (1970).

⁷E. D. Palik and R. Bray, Phys. Rev. B **3**, 3302 (1971).

⁸J. K. Wajda and R. Bray, in *Proceedings of the Twelfth International Conference on the Physics of Semiconductors* (Teubner, Stuttgart, 1974), p. 877.

⁹C. C. Lee and H. Y. Fan, Phys. Rev. B **9**, 3502 (1974).

¹⁰G. K. Celler, S. Mishra, and R. Bray, Appl. Phys. Lett. **27**, 297 (1975).

¹¹D. A. Abramsohn, G. K. Celler, and R. Bray, in *Proceedings of the International Conference on Optical Properties of Highly Transparent Solids, New Hampshire, 1975*, edited by S. S. Mitra and E. Bendow (Plenum, New York), p. 221.

¹²G. K. Celler and R. Bray, Appl. Phys. Lett. **27**, 53 (1975).

¹³A. R. Hutson and D. L. White, J. Appl. Phys. **33**, 40 (1962).

¹⁴D. L. White, J. Appl. Phys. **33**, 2547 (1962).

¹⁵H. D. Nine, Phys. Rev. Lett. **4**, 359 (1960); A. R. Hutson, *ibid.* **4**, 505 (1960); for review see J. H.

McFee, in *Physical Acoustics*, edited by W. P. Mason (Academic, New York, 1966), Vol. IV, part A, p. 1. It should be noted that control of the carrier concentration by dc photoconductive effect in semi-insulating materials, such as CdS, has been used to influence the generation of acoustoelectric instabilities and the domain formation.

¹⁶G. Weinreich, *Phys. Rev.* **107**, 317 (1957).

¹⁷D. L. Spears and R. Bray, *Phys. Lett. A* **29**, 542 (1969).

¹⁸International Laser Systems, Inc., Model NT-50/50p Laser, which was loaned to us by Dr. E. D. Palik.

¹⁹At room temperature the carrier mobility is rela-

tively insensitive to impurity scattering.

²⁰The longitudinal case including absorption has been solved, but as we do not attempt a quantitative analysis of the experimental results, it is advantageous for clarity of discussion to describe only the simplified models.

²¹For a review of controversy regarding alternative definitions of γ see R. Bray, in *Proceedings of the Tenth International Conference on the Physics of Semiconductors*, edited by S. P. Keller, J. C. Hensel, and F. Stern (U. S. AEC Div. of Tech. Information, Oak Ridge, Tenn., 1970) p. 705; also N. I. Meyer and M. H. Jorgensen, Ref. 3 above.

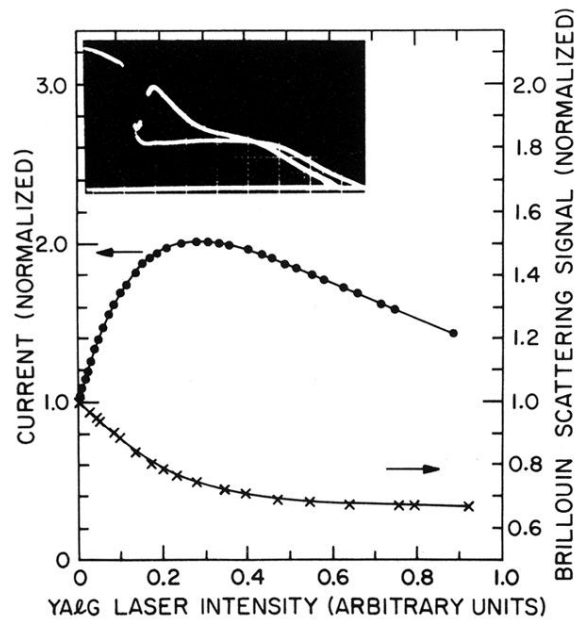


FIG. 7. Current and Brillouin scattering curves in the t_3 regime, as a function of the peak laser light intensity in longitudinal geometry. The scattering curve is for 0.8-GHz phonons. Photograph in the insert shows two persistent current traces, one in the dark, another with the laser pulse illumination of the intensity chosen to maximize the current increase. Note also that after illumination the current decays faster.

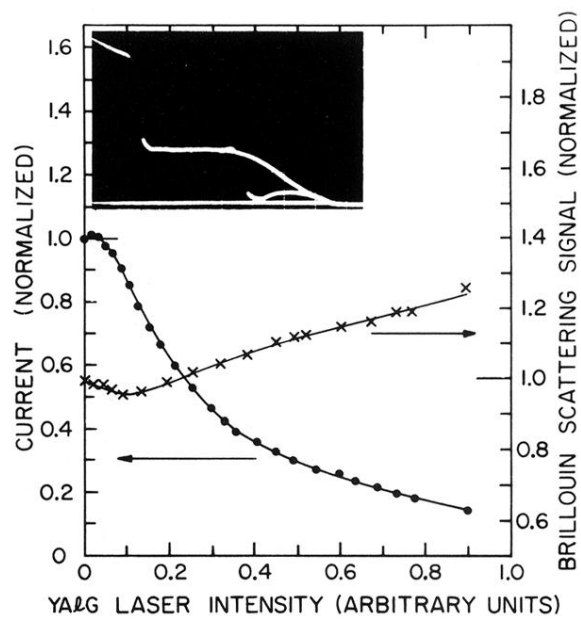


FIG. 8. Current and Brillouin scattering curves in the t_4 regime, as a function of the peak laser light intensity in longitudinal geometry. The scattering curve is for 0.8-GHz phonons. Photograph in the insert shows two persistent current traces, one in the dark, another with the laser pulse of the maximum intensity available.

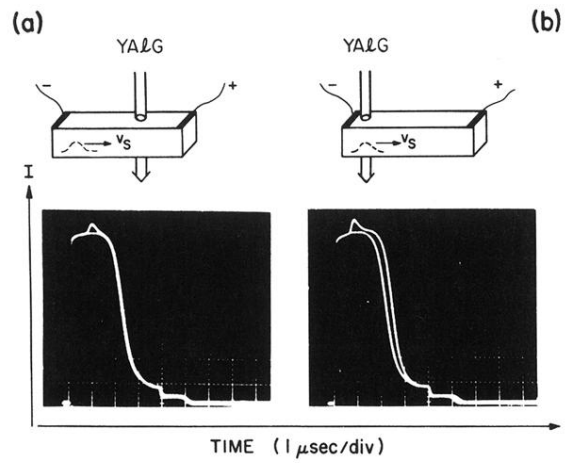


FIG. 9. Current modulation effects for light incident on the sample in the t_1 regime in transverse geometry. (a) Position of the light beam does not coincide with the location of the embryonic domain. Only a small current spike is observed. (b) Light beam illuminates the embryonic domain. In addition to the current spike, there is an increase in the incubation time of the domain.